[^{225}Ac]Ac-PSMA I&T: A Preclinical Investigation on the Fate of Decay Nuclides and Their Influence on Dosimetry of Salivary Glands and Kidneys

Alexander Wurzer[1], Baiqing Sun[1], Samaa Saleh[1,2], Julia Brosch-Lenz[1], Sebastian Fischer[1], Susanne Kossatz[1], Kerstin Hürkamp[2], Wei Bo Li[2], Matthias Eiber[1], Alfred Morgenstern[3], Frank Bruchertseifer[3], Wolfgang Weber[1], and Calogero D'Alessandria[1]

[1]*Nuklearmedizinische Klinik und Poliklinik, Klinikum rechts der Isar, Technical University of Munich, München, Germany;* [2]*Institute of Radiation Medicine, Helmholtz Zentrum München, German Research Center for Environmental Health, Neuherberg, Germany; and* [3]*Joint Research Centre, European Commission, Karlsruhe, Germany*

α-therapy with ^{225}Ac-labeled radioligands targeting prostate-specific membrane antigen (PSMA) has emerged as a promising treatment option for advanced metastatic castration-resistant prostate cancer. Because of α-recoil, the progeny is released from the PSMA-targeted molecule and can undergo redistribution, contributing to off-target toxicity. Here, we report on biodistribution and dosimetry studies of [^{225}Ac]Ac-PSMA I&T performed in mice to investigate the pharmacokinetics of the radioligand compared with unbound progeny. Moreover, the cellular uptake and externalization kinetics of [^{225}Ac]Ac-PSMA I&T were compared with those of its ^{177}Lu-labeled analog. **Methods:** In vitro studies were performed on LNCaP and PC3 PIP cells. Biodistribution studies (performed 10 min to 7 d after injection) were conducted in LNCaP tumor–bearing and healthy mice. Equilibrium uptake was determined 24 h after dissection by quantification of ^{221}Fr (218 keV) and ^{213}Bi (440 keV). Tissues of interest (kidneys, salivary glands, and tumor tissue) were measured immediately after dissection until reaching equilibrium to determine the time-dependent activity distribution of ^{221}Fr and ^{213}Bi. Absorbed doses were calculated using MIRDcalc, assuming decay of the progeny at the site of the first decay versus taking into account redistribution of unbound progeny. **Results:** [^{225}Ac]Ac-PSMA I&T demonstrated cell-binding characteristics and cellular retention similar to those of [^{177}Lu]Lu-PSMA I&T. In biodistribution studies, no redistribution of ^{221}Fr and ^{213}Bi was measured from tumor tissue. Higher uptake of ^{213}Bi was found in the kidneys (2-fold higher at 10 min and at 1 h after injection) and salivary glands (1.7-fold and 8.5-fold higher at 10 min and 1 h after injection, respectively) at the time of death compared with equilibrium. This contribution increased the absorbed dose in the kidneys and salivary glands by a factor of 1.3 and 2.5, respectively, assuming uptake of ^{221}Fr and in situ formation of ^{213}Bi. **Conclusion:** The PSMA-targeting characteristics and pharmacokinetics of [^{225}Ac]Ac-PSMA I&T are similar to those of [^{177}Lu]Lu-PSMA I&T. The progeny of [^{225}Ac]Ac-PSMA I&T is trapped in tumor tissue. Uptake of liberated decay products into the salivary glands and kidneys was identified as an additional factor explaining the increased side effects of ^{225}Ac therapy compared with ^{177}Lu-based radioligands.

Key Words: PSMA; TAT; α-therapy; radionuclide therapy; radiochemistry

J Nucl Med 2025; 66:1964–1969
DOI: 10.2967/jnumed.125.269744

The α-emitter ^{225}Ac shows promise for prostate-specific membrane antigen (PSMA)–targeted therapy of metastatic castration-resistant prostate cancer (*1*). The 2 most frequently applied radioligands for targeted α-therapy (TAT)—PSMA-617 and PSMA I&T—are expected to have a similar efficacy on the basis of retrospective studies (*2*,*3*). [^{225}Ac]Ac-PSMA I&T and [^{225}Ac]Ac-PSMA-617 are currently being evaluated in prospective clinical trials and are applied under compassionate use for the treatment of patients with metastatic castration-resistant prostate cancer and refractory to [^{177}Lu]Lu-PSMA therapy (*1*).

TAT was found to reduce prostate-specific antigen levels by more than 50% in 50%–65% of heavily pretreated patients, depending on patient selection criteria (*1*–*3*), and by more than 90% in 82% of chemotherapy-naïve patients (*4*). The elevated radiobiologic effect of α-emitters bears potential risks for healthy tissues. One of the most common side effects of ^{225}Ac TAT is permanent grade 1–3 xerostomia (*1*). The accompanying reduction in quality of life results in discontinuation of treatment in a significant portion of patients, despite their response to treatment (*2*). Although an overall tolerable toxicity profile was found in retrospective studies, with a modest level of hematologic and renal toxicity (*1*), data on long-term side effects are scarce and warrant further evaluation, especially when applying ^{225}Ac TAT in earlier lines of treatment.

^{225}Ac has a half-life of 9.9 d and decays by emission of 4 α- and 2 β-particles (Fig. 1). Once the first α-particle is emitted, a recoil effect occurs, liberating the daughter nuclide (^{221}Fr) from the PSMA-targeting vector (*5*). Unbound ^{221}Fr and its nonbound decay nuclides can potentially redistribute and contribute to off-target toxicity. In previous dosimetry estimates, it was assumed that all daughter nuclides decay at the site of the first α-decay without any relevant relocation (*6*).

In the present study, we aimed to determine the fate of the daughter nuclides of a single injection of [^{225}Ac]Ac-PSMA I&T in biodistribution studies of healthy and tumor-bearing mice. Organs of interest were measured immediately after dissection at multiple time points by quantification of the γ-energies of ^{221}Fr and ^{213}Bi until reaching a secular equilibrium with ^{225}Ac. Three scenarios

Received Feb. 18, 2025; revision accepted Sep. 5, 2025.
For correspondence, contact Calogero D'Alessandria (calogero.dalessandria@tum.de).
Published online Oct. 3, 2025.

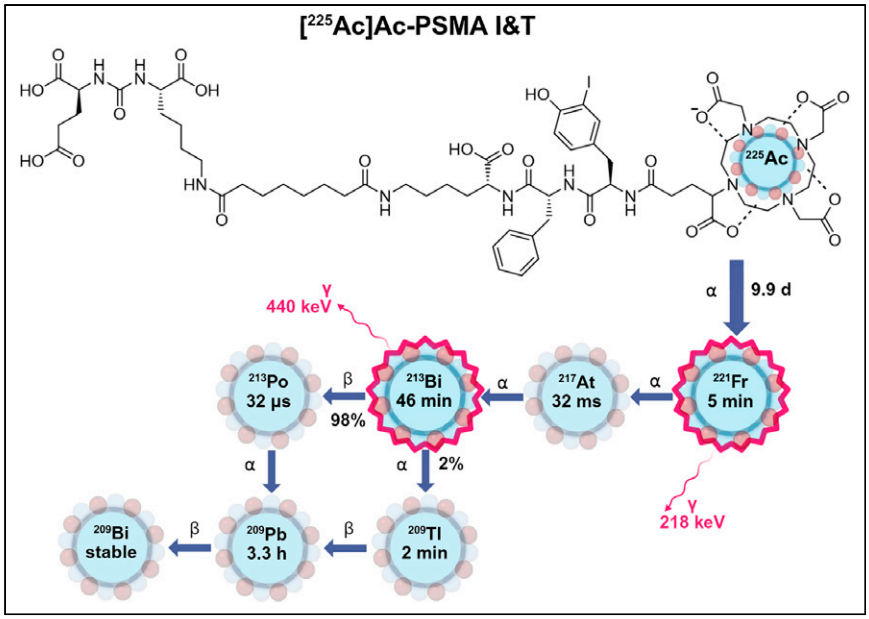

FIGURE 1. Structural formula of [^{225}Ac]Ac-PSMA I&T and decay nuclides.

were considered. If uptake at the time of dissection was higher than at equilibrium, this would suggest accumulation of unbound, nonequilibrium nuclides within the organ. If uptake was lower, it would indicate rapid delocalization of the liberated progeny from the tissue after the first decay. Finally, if the count rate remained constant, it would imply that the decay products stayed trapped within the organ at the site of the first decay. The biodistribution studies were accompanied by a detailed in vitro characterization of the cell uptake and cellular retention kinetics of [^{225}Ac]Ac-PSMA I&T versus [^{177}Lu]Lu-PSMA I&T.

MATERIALS AND METHODS

Details on lipophilicity measurements and cell culture are provided in the supplemental materials, available at http://jnm.snmjournals.org.

Radiolabeling

^{225}Ac was provided by the Joint Research Centre of the European Commission. The radionuclidic and radioisotopic purities of ^{225}Ac exceeded 99.98% for all batches, according to the certificate of analysis. Quality control of the ^{225}Ac produced from a ^{229}Th source included α- and γ-spectrometry and inductively coupled plasma mass spectrometry, as described previously (*7*). Radiolabeling with ^{225}Ac and quality control was performed as previously described (*8*). Further details on the labeling protocol and quality control procedures are provided in the supplemental materials. Labeling of PSMA I&T with ^{177}Lu and quality control were performed in accordance with established procedures (*9*).

Affinity Studies

Competitive binding studies were performed on LNCaP cells (1.5×10^5 cells per well). Because of the absence of a nonradioactive ^{225}Ac isotope, the studies were performed using an inverse approach, as previously described (*10*), using natural Lu-PSMA I&T as a reference radioligand in increasing concentrations (10^{-5}–10^{-11} M per well; $n = 3$ each), whereas the radioligands were applied in a concentration of 5.0 nM per well. In this inverse experimental approach, higher inhibitory concentration of 50% values corresponded with higher affinities (inverse inhibitory concentration of 50%).

Internalization Studies

Internalization of the radiolabeled radioligands (5.0 nM per well) was determined on PC3 PIP and LNCaP cells (1.5×10^5 cells per well) at 37 °C after 30 and 60 min ($n = 3$), as previously described (*10*). Surface-bound radioligand was removed by a washing step with excess of 2-phosphonomethyl pentanedioic acid (PMPA) (MedChemExpress). Unspecific internalization was determined in a parallel blockade experiment ($n = 3$) by incubation of the radioligand in excess PMPA. The amount of internalized activity was corrected for surface-bound and nonspecifically internalized radioligand.

Externalization Studies

Cellular retention of the PSMA radioligands in PC3 PIP cells (1.5×10^5 cells per well) was determined after 60, 120, and 180 min ($n = 3$). After the incubation period (5.0 nM per well for 1 h at 37 °C), the supernatant with unbound free radioligand was removed and fresh assay medium was added. Cellular retention was determined in 2 experimental conditions: 37 °C alone and 37 °C with blocking of reinternalization with molar excess of PMPA. In each condition, surface-bound radioligand was removed by PMPA. The remaining internalized fraction was determined after lysis and normalized to the internalized fraction after 60 min of incubation.

Animals and Tumor Xenograft Model

All animal experiments were conducted in accordance with the general animal welfare regulations in Germany (approval 55.2-1-54–2532-216-2015) and the institutional guidelines for the care and use of animals. Biodistribution studies were conducted in 6- to 8-wk-old, healthy, male C57BL/6 mice and LNCaP tumor–bearing SCID mice (Charles River Laboratories) (*10*). Animals with a tumor diameter of greater than 0.5 cm were used for the experiments.

Biodistribution Studies

Biodistribution of the radioligand was investigated in groups ($n = 5$) of healthy and LNCaP tumor–bearing mice after 10 min, 1 h, 24 h, and 7 d. [^{225}Ac]Ac-PSMA I&T (72 ± 8 kBq, 1 nmol) in isotonic saline was injected via catheter into the tail vein of animals under isoflurane anesthesia. At 10 min, 1 h, and 24 h after injection, organs of interest in tumor-bearing mice (kidneys, submandibular glands, and tumors) were excised, weighed, and measured immediately after dissection in a γ-counter, by separate quantification of the γ-energies of ^{221}Fr and ^{213}Bi. These measurements were repeated multiple times until reaching equilibrium. All organs were remeasured at approximately 24 h after dissection to ensure equilibrium between ^{225}Ac and its progeny.

Counts per minute were corrected for background radiation and adjusted for radioactive decay to the time of injection using the half-life of ^{225}Ac. Uptake of [^{225}Ac]Ac-PSMA I&T at equilibrium was expressed as a percentage of the injected activity per gram of tissue. Nonequilibrium data were normalized to the uptake value of the specific organ at equilibrium and presented as a percentage of uptake at equilibrium (UEQ). The UEQs of the organs of interest ($n = 5$ per group) and the time interval between γ-counter measurement and sacrifice of the mouse were plotted until equilibrium was achieved.

Dosimetry Calculations

The time-integrated activity coefficients for [^{225}Ac]Ac-PSMA I&T were calculated using the biodistribution data in tumor-bearing

animals, as described previously (*11*). Normal organ radiation doses were estimated for a 73-kg standard adult anatomic model using the time-dependent organ activity accumulation and the total-body activities measured in the biodistribution studies (*12*). Tissue activity concentrations were converted to fractional activities in the standard 73-kg adult by considering the relative organ masses between the standard adult and the 25-g mouse. The relative biologic efficacy for the α-particles was assumed to be 5 (*6*). Absorbed dose values were calculated with MIRDCalc version 1.21 (Genesis) (*13*). To calculate the impact of nonequilibrium progeny on the absorbed dose of the salivary glands and kidneys, the time-integrated activity coefficients of equilibrium and nonequilibrium uptake were determined by numeric integration using the trapezoidal rule. Respective deltas were determined, and absorbed dose values were calculated for 2 scenarios: either accumulation of nonequilibrium ^{221}Fr (scenario 1, with 3 of 4 α-decays in organs at risk) or ^{213}Bi (scenario 2, with 1 of 4 α-decays in organs at risk). Dosimetry data were generated using the equilibrium and nonequilibrium data of ^{213}Bi. The calculations for ^{221}Fr (scenario 1) assumed that all nonequilibrium ^{213}Bi was in situ generated from ^{221}Fr within the organ of interest. Moreover, the impact of the presence of 10% of [^{213}Bi]Bi-PSMA I&T, which could form as a side product during radiolabeling, on the dosimetry was calculated (supplemental materials).

RESULTS

Radiolabeling

Radiochemical yield, determined by radio–thin layer chromatography, of [^{225}Ac]Ac-PSMA I&T at the end of synthesis was 98.4% ± 1.0%. After radiosynthesis and formulation, injection of all animals in a group was completed in 1.5–3.5 h. Over this time span, radiochemical purity by radio–thin layer chromatography of the formulated product decreased to 95.5 ± 0.6% at 4 h after synthesis. Radiochemical purity, as determined by high-performance liquid chromatography, was 99% or greater after radiosynthesis and 95.0% or greater at 4 h after synthesis, with fraction-based quantification of the eluate in a γ-counter (representative chromatograms provided in Supplemental Fig. 1). Radiochemical yield and radiochemical purity of [^{177}Lu]Lu-PSMA I&T were 97% or greater.

In Vitro Characterization

^{225}Ac-labeled PSMA I&T was slightly less hydrophilic than [^{177}Lu]Lu-PSMA I&T, with log D (octanol and phosphate-buffered saline, pH 7.4) values of −3.7 ± 0.2 and −4.1 ± 0.1, respectively. Both compounds demonstrated a comparable and high binding affinity to PSMA and similar internalization kinetics into PSMA-expressing cells. Uptake into LNCaP cells was approximately 3-fold lower than in PC3 PIP cells. In the cellular retention assay, which mimics the in vivo situation by allowing reinternalization, both radioligands had a cellular retention of approximately 60% after 180 min. By blocking reinternalization, cellular retention dropped to 15% for both radioligands (Fig. 2; Supplemental Table 1).

In Vivo Characterization

Considering the relatively large fraction of noninternalized radioligand after 180 min in the cellular in vitro models, we aimed to further investigate the distribution of [^{225}Ac]Ac-PSMA I&T and the ^{225}Ac-derived progeny (^{221}Fr and ^{213}Bi) in mouse models.

Biodistribution at Equilibrium. All organs were measured 24 h after dissection, meaning that nonequilibrium daughter nuclides had already decayed and uptake values corresponded solely to the distribution of [^{225}Ac]Ac-PSMA I&T. The biodistribution data were acquired by quantification of the γ-emission of ^{221}Fr (Fig. 3) and ^{213}Bi (Supplemental Fig. 2; Supplemental Table 2). At 10 min after injection, the maximum tumor uptake of approximately 5 %IA/g was reached. Analogous to the in vitro experiments, 60% of the activity was retained in the tumor tissue after 24 h over 7 d. After 10 min, most off-target tissues (e.g., submandibular glands) displayed a similar uptake as measured in the blood pool, ranging from 1 to 4 %IA/g, with rapid excretion during the first hour. Pronounced excretion of the radioactivity occurred via the kidneys, with a maximum uptake of 25 %IA/g at 10 min and rapid clearance kinetics within 24 h (≤3.5 %IA/g). In tumor-bearing animals, a fraction of the activity accumulated in the liver (2 %IA/g) and was not cleared within 7 d. In contrast, the activity in the liver of healthy animals cleared within the first hour to less than 0.7 %IA/g. With this exception, the overall distribution pattern was similar between healthy and tumor-bearing animals. No significant differences in distribution were found between ^{221}Fr and ^{213}Bi.

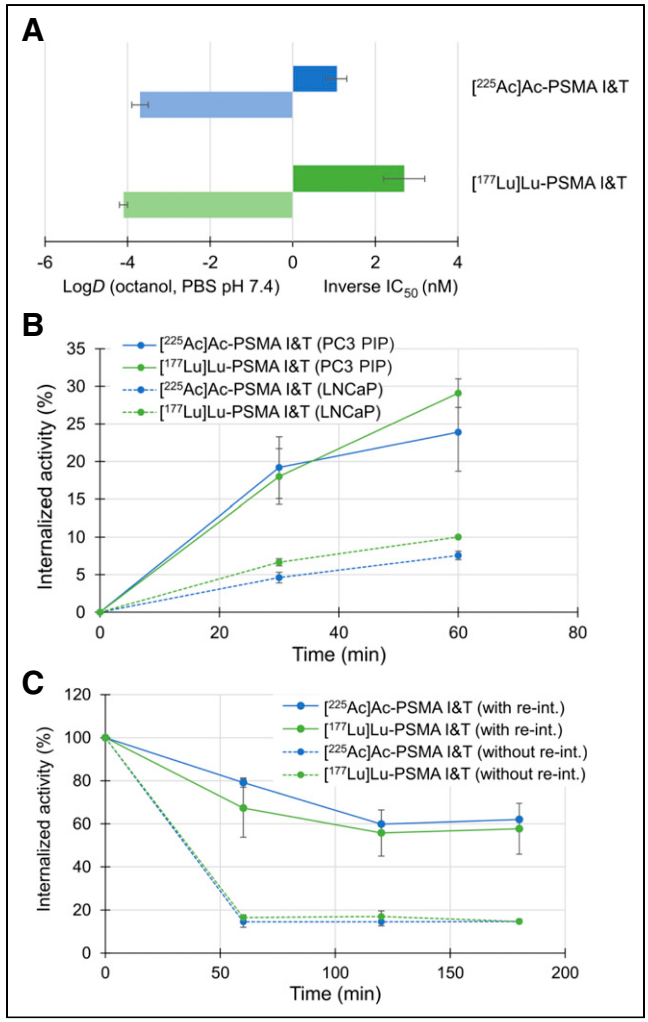

FIGURE 2. In vitro characteristics of [^{225}Ac]Ac-PSMA I&T (blue) and [^{177}Lu]Lu-PSMA I&T (green). (A) Lipophilicity expressed as partition coefficient (log *D*) in octanol and phosphate-buffered solution (PBS) pH 7.4 (n = 6) and binding affinities (inverse IC_{50}; 1 h, 4°C, n = 3). (B) Internalization kinetics into PC3 PIP cells (solid lines) and LNCaP cells (dashed lines) at 37°C, over 60 min (n = 3). (C) Cellular retention in PC3 PIP cells over 180 min at 37°C, with reinternalization (re-int.) (solid lines) and blocking of reinternalization (dashed lines) by molar excess of PMPA (n = 3). Data are presented as mean ± SD. IC_{50} = inhibitory concentration of 50%.

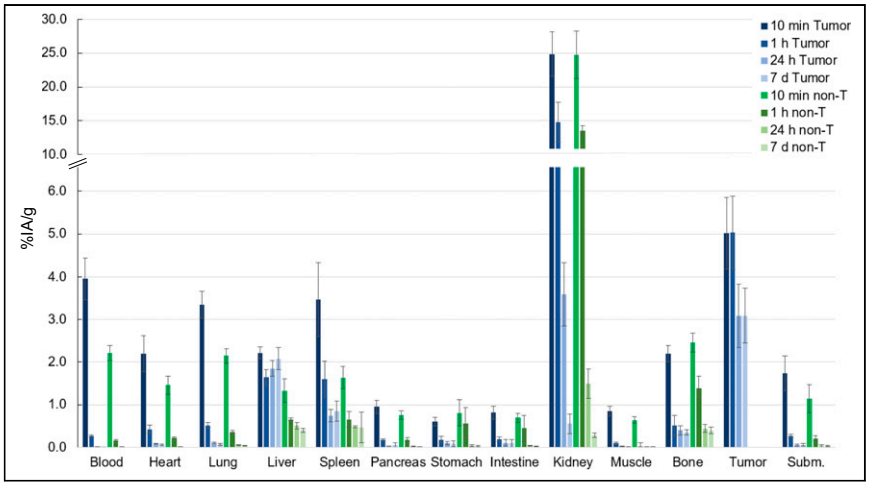

FIGURE 3. Biodistribution of [^{225}Ac]Ac-PSMA I&T in LNCaP tumor–bearing (blue) and healthy animals (green) at 10 min, 1 h, 24 h, and 7 d after injection. Samples were measured 24 h after dissection in γ-counter by quantification of ^{221}Fr. Data are expressed as mean ± SD percentage of injected activity per gram (n = 5). Subm. = submandibular glands.

Nonequilibrium Biodistribution. The UEQ describes the percentage change in uptake of ^{221}Fr and ^{213}Bi at multiple time points after dissection compared with equilibrium. On average, 20–30 min elapsed between the time of death and the measurement of the first organ in the γ-counter.

^{213}Bi uptake in the kidneys at 10 min and 1 h after injection was 1.8- and 2-fold higher at the time of death compared with equilibrium, respectively (Figs. 4A and 4B). No differences in uptake were found in the kidneys at 24 h after injection. Uptake of ^{213}Bi in the submandibular glands at 10 min and 1 h after injection was approximately 1.7- and 8.5-fold higher at the time of death, respectively, corresponding to 2.9 and 2.2 %IA/g, compared with the equilibrium uptake of 1.7 and 0.3 %IA/g (Figs. 4C and 4D). Because of the rapid washout of [^{225}Ac]Ac-PSMA I&T from murine salivary glands (<0.1 %IA/g), no analysis was performed at 24 h after injection. ^{213}Bi uptake remained constant in tumor tissue at all time points (Supplemental Fig. 3).

The uptake of short-lived ^{221}Fr remained nearly constant after dissection until reaching equilibrium in the kidneys and tumor tissue, reflected by a mean UEQ of approximately 100% ± 10%. In the salivary glands, the trends were less pronounced compared with the distribution of ^{213}Bi (Supplemental Fig. 4).

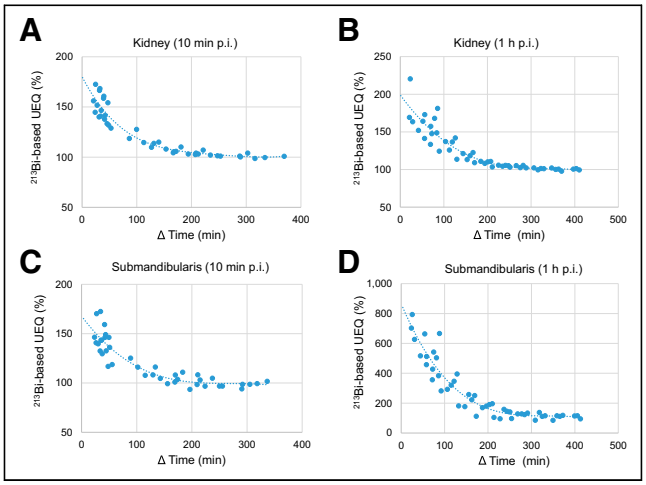

FIGURE 4. ^{213}Bi uptake compared with equilibrium (UEQ). Percentage change of ^{213}Bi uptake in kidneys at 10 min after injection (A) and 1 h after injection (B), and submandibular glands at 10 min after injection (C) and 1 h after injection (D), compared with respective uptake at equilibrium. Samples (n = 5) were measured at multiple time points until reaching equilibrium. Δ Time = difference between time of measurement in γ-counter and time of sacrifice of mouse; p.i. = postinjection.

Dosimetry Calculations. Using the data from mice at equilibrium, the absorbed dose of [^{225}Ac]Ac-PSMA I&T in the kidneys and salivary glands was 1.11 and 0.20 Sv_{RBE5}/MBq, respectively. These values reflect instant decay of the daughter nuclides without translocation. All other equilibrium values are summarized in Supplemental Table 3. Time-integrated activity coefficients were 135% and 295% higher in the kidneys and salivary glands, respectively, with additionally considering nonequilibrium distribution compared with equilibrium alone. For the kidneys, this would result in an absorbed dose of 1.40 Sv_{RBE5}/MBq, assuming accumulation of nonequilibrium ^{221}Fr until decay to stable ^{209}Bi. When translocation of ^{213}Bi only is assumed, the absorbed dose in the kidneys would increase to 1.21 Sv_{RBE5}/MBq. Regarding nonequilibrium uptake in the salivary glands, the absorbed dose would increase to 0.50 and 0.30 Sv_{RBE5}/MBq for accumulation of nonequilibrium ^{221}Fr (3 additional α-decays) and ^{213}Bi (1 additional α-decay), respectively. The potential presence of 10% of [^{213}Bi]Bi-PSMA I&T in the formulation had no significant impact on the absorbed doses (supplemental materials).

DISCUSSION

Currently, TAT with [^{225}Ac]Ac-PSMA is most often used for treatment of metastatic castration-resistant prostate cancer after extensive pretreatment with novel antiandrogens, chemotherapy, and ^{177}Lu radiopharmaceutical therapy (*1*). The higher linear energy transfer of an α-particle, compared with ^{177}Lu, results in a 4.2-fold greater relative biologic effectiveness of [^{225}Ac]Ac-PSMA I&T compared with [^{177}Lu]Lu-PSMA I&T and allows for the treatment of highly resistant tumor cells (*14*).

Because of the elevated cytotoxicity of [^{225}Ac]Ac-PSMA I&T, we investigated the in vivo distribution of [^{225}Ac]Ac-PSMA I&T in healthy and tumor-bearing mouse models, with a focus on the distribution of nonequilibrium daughter nuclides.

In cell assays, [^{225}Ac]Ac-PSMA I&T and [^{177}Lu]Lu-PSMA I&T showed comparable binding affinities and uptake kinetics in LNCaP and PC3 PIP cells, indicating that the increased relative biologic effectiveness of the α-emitting radioligand is due to the radionuclide's properties and not influenced by different cell-binding characteristics arising from the different complex structures. These results align with a previous in vitro comparison of both radioligands on PC3 PIP cells (*14*). The lower internalization rate into LNCaP cells compared with that of PC3 PIP cells can be explained with the approximately 10-fold lower number of PSMA binding sites on LNCaP cells versus PC3 PIP cells (*15*).

The overall distribution profile of [^{225}Ac]Ac-PSMA I&T, distinguished by rapid clearance from the blood pool (mainly via the

renal system and rapid tumor uptake), can be compared with that of [^{177}Lu]Lu-PSMA I&T, reported by our group in a previous study using the same xenograft model (*11*). In that study, [^{177}Lu]Lu-PSMA I&T displayed an 11- and 22-fold higher uptake in the kidneys at 1 h (166 ± 21 IA/g) and 24 h and (77 ± 23 %IA/g), respectively, compared with the [^{225}Ac]Ac-PSMA I&T data found in the current study (15 ± 3 and 4 ± 1 %IA/g at 1 and 24 h after injection, respectively) (*11*). This finding can be explained by the 25-fold higher amount of peptide injected in the current study, arising from the different molar activity of [^{225}Ac]Ac-DOTA–based molecules (0.1–0.2 MBq/nmol) (*16*) compared with their ^{177}Lu-labeled counterparts (30–50 MBq/nmol) (*17*). Injection of formulations with a low molar activity has been found to reduce kidney uptake of PSMA-targeted molecules (*18*,*19*). Liver uptake was increased by up to 5-fold in tumor-bearing animals compared with healthy controls, supporting the assumption that the radioligand is metabolized in tumor tissue and that ^{225}Ac or other lipophilic metabolites accumulate in the liver (*20*). Elevated uptake of [^{225}Ac]Ac-PSMA-617 in the liver was also found in tumor-bearing animals, whereas the uptake of the ^{177}Lu-labeled version in the liver was minor (*21*).

The salivary glands are considered a main dose-limiting organ for PSMA TAT. The molecular mechanism of PSMA radioligand uptake into the salivary glands is not completely understood. Because endogenous PSMA expression is considerably lower than empiric PSMA radioligand uptake would account for (*22*), possible uptake mechanisms include an affinity to glutamate carboxypeptidase III (*23*) and ion-transporter or transporter-independent systems (*24*). Results from the current study indicate that salivary gland uptake of liberated progeny may contribute to the increased salivary gland toxicity of [^{225}Ac]Ac-PSMA compared with that of ^{177}Lu-labeled analogs. The effect of unbound progeny significantly increased the absorbed dose in the salivary glands by a factor of 1.5 (uptake of ^{213}Bi, 1 additional α-decay) to 2.5 (uptake of ^{221}Fr, 3 additional α-decays). It is noteworthy that the salivary gland values at equilibrium (0.20 Sv_{RBE5}/MBq) are more than 10-fold lower than those calculated by Kratochwil et al. using human data (2.33 Sv_{RBE5}/MBq) (*6*). This can be explained by the significantly lower uptake of PSMA radioligands in mice versus humans (*25*).

Unbound ^{213}Bi is known for its clearance via the renal system (*26*). To the best of our knowledge, no data are available on its accumulation in the salivary glands. Early work investigating the distribution of monovalent ^{221}Fr described its accumulation in the salivary glands of rats (*27*), which may help to explain the in situ presence of elevated levels of unbound ^{213}Bi deriving from ^{221}Fr.

Our absorbed dose for the kidneys at equilibrium (1.11 Sv_{RBE5}/MBq) falls in a similar range as previously determined for [^{225}Ac]Ac-PSMA-617 (0.74 Sv_{RBE5}/MBq), using human data from the ^{177}Lu compound (*6*). For the kidneys, the additional uptake of nonequilibrium nuclides only moderately increased the absorbed dose by an average factor of 1.1–1.3, corresponding to 1.21–1.40 Sv_{RBE5}/MBq. Our findings of increased renal uptake align with results from a study performed with a small patient cohort (n = 5) using quantitative posttreatment ^{221}Fr/^{213}Bi-based SPECT/CT after PSMA TAT (*28*). Here, the kidney SUV ratio of ^{213}Bi compared with that of ^{221}Fr increased by 9 ± 8% over time, indicating a non-PSMA–driven behavior of ^{213}Bi as a result of redistribution and renal excretion, whereas ^{221}Fr was concluded to remain at the site of the first decay (*28*).

The apparent absence of nonequilibrium ^{213}Bi salivary gland uptake at 24 h after injection is likely a result of the rapid clearance of the radioactivity from the organism. After 24 h, significant uptake (1–4 %IA/g) was found solely in the liver, kidneys, and tumor tissue, cumulatively corresponding to approximately 2.0 kBq, which makes it nearly impossible to assess potential redistribution. With a mean time of 20–30 min from time of death to the first measurement of resected tissues in the γ-counter, it is less surprising that no significant amount of nonequilibrium ^{221}Fr was detected after 4–6 half-lives.

Importantly, the absence of redistribution of ^{221}Fr and ^{213}Bi from tumor tissue in this preclinical model suggests that the effectiveness of ^{225}Ac TAT relies on cumulative energy transfer by ^{225}Ac and its α-emitting progeny. Apart from redistribution, the effects of ^{225}Ac progeny present in the formulation need to be considered. Secular equilibrium with ^{225}Ac is established after approximately 6 half-lives of the respective daughter nuclide, meaning that a dose of [^{225}Ac]Ac-PSMA I&T contains almost the identical amount of activity of ^{221}Fr, ^{217}At, ^{213}Bi, and ^{213}Po at 4.5 h after synthesis (*29*). Despite the short half-lives of ^{225}Ac progeny, their distribution will most likely increase the absorbed dose to off-target tissues. In the current study, effects from daughter nuclides in the formulation are negligible on the nonequilibrium uptake found in the salivary glands and kidneys, owing to the constant high uptake in these tissues between 10 min and 1 h after injection. Pentetic acid is often added as a chelator to clinical formulations of ^{225}Ac-based pharmaceuticals to promote their excretion (*8*). However, no studies are available on beneficial effects on clearance kinetics.

A general limitation of the current study is the low injected activity (<0.1 MBq), which is prone to errors because of the effects from background radiation and limits of quantification in the γ-counter. Because of the short half-lives of the α-emitting progeny in combination with rapid excretion of [^{225}Ac]Ac-PSMA I&T from mice at 24 h after injection, assessment of nonequilibrium distribution remains challenging, especially for ^{221}Fr and at later time points. The dosimetry calculation, considering the accumulation of nonequilibrium ^{221}Fr, assumed that the measured nonequilibrium ^{213}Bi was formed in situ from nonequilibrium ^{221}Fr within the organ of interest. Moreover, differences between murine and human organs can affect the distribution of nonequilibrium nuclides within the organism.

CONCLUSION

[^{225}Ac]Ac-PSMA I&T demonstrated cell-binding characteristics and pharmacokinetics similar to those of its ^{177}Lu-labeled analog, which is reassuring for its clinical use. The α-emitting progeny of ^{225}Ac remained trapped in tumor tissue, explaining the high efficacy of PSMA TAT. ^{213}Bi formed by α-recoil accumulated in the salivary glands and renal system, resulting in an increased absorbed dose to the organs at risk. The effect of unbound progeny to the development of xerostomia and potential long-term side effects on the renal system warrant further investigation.

DISCLOSURE

This work was supported by a grant from the German Bundesamt für Strahlenschutz (grant 3621S42440) and by a Young Investigator Award to Alexander Wurzer from the CRIS Cancer and Prostate Cancer Foundation. Alexander Wurzer and Matthias Eiber are listed as inventors in patent applications for rhPSMA and entitled to royalties on sales of POSLUMA. Matthias Eiber reports fees from Blue Earth Diagnostics (consultant, research funding), Novartis/AAA (consultant, speaker), Telix Pharmaceuticals (consultant), Bayer (consultant, research funding), RayzeBio (consultant), Point Biopharma (consultant), Eckert-Ziegler (speaker),

Janssen Pharmaceuticals (consultant, speakers bureau), Parexel (image review), and Bioclinica (image review) outside the submitted work. Wolfgang Weber reports research support from Siemens Healthineers, Blue Earth Diagnostics, ITM, Novartis, Pentixapharm, Ratio Therapeutics, RayzeBio, Trimt, and Roche; serves as employee, consultant, and/or stockholder of Immu-Veo, ITM, Novartis, RayzeBio, and Roche; reports honoraria from Siemens Healthineers; and serves on the scientific advisory board of Immune-Image and Immu-Veo. Calogero D'Alessandria declares research support from Blue Earth Therapeutics and serves as consultant, stockholder, and advisory board member of Immu-Veo. No other potential conflict of interest relevant to this article was reported.

ACKNOWLEDGMENTS

We thank Natalie Röder and Markus Mittelhäuser for their technical assistance.

KEY POINTS

QUESTION: Do decay nuclides liberated during ^{225}Ac TAT of metastatic castration-resistant prostate cancer contribute to toxicity in the salivary glands and kidneys?

PERTINENT FINDINGS: In this preclinical study, liberated decay nuclides were found to accumulate in murine salivary glands and kidneys, resulting in an increased absorbed dose in these organs. No redistribution was found from tumor tissue, explaining the high efficacy of TAT.

IMPLICATIONS FOR PATIENT CARE: Strategies promoting the excretion of decay nuclides during ^{225}Ac TAT could reduce risks for the development of xerostomia or renal impairment in patients receiving this therapy.

REFERENCES

1. Sathekge MM, Lawal IO, Bal C, et al. Actinium-225-PSMA radioligand therapy of metastatic castration-resistant prostate cancer (WARMTH Act): a multicentre, retrospective study. *Lancet Oncol.* 2024;25:175–183.
2. Feuerecker B, Tauber R, Knorr K, et al. Activity and adverse events of actinium-225-PSMA-617 in advanced metastatic castration-resistant prostate cancer after failure of lutetium-177-PSMA. *Eur Urol.* 2021;79:343–350.
3. Zacherl MJ, Gildehaus FJ, Mittlmeier L, et al. First clinical results for PSMA-targeted α-therapy using ^{225}Ac-PSMA-I&T in advanced-mCRPC patients. *J Nucl Med.* 2021;62:669–674.
4. Sathekge M, Bruchertseifer F, Knoesen O, et al. ^{225}Ac-PSMA-617 in chemotherapy-naive patients with advanced prostate cancer: a pilot study. *Eur J Nucl Med Mol Imaging.* 2019;46:129–138.
5. Thiele NA, Wilson JJ. Actinium-225 for targeted α therapy: coordination chemistry and current chelation approaches. *Cancer Biother Radiopharm.* 2018;33:336–348.
6. Kratochwil C, Bruchertseifer F, Rathke H, et al. Targeted α-therapy of metastatic castration-resistant prostate cancer with ^{225}Ac-PSMA-617: dosimetry estimate and empiric dose finding. *J Nucl Med.* 2017;58:1624–1631.
7. Apostolidis C, Molinet R, Rasmussen G, Morgenstern A. Production of Ac-225 from Th-229 for targeted alpha therapy. *Anal Chem.* 2005;77:6288–6291.
8. Hooijman EL, Chalashkan Y, Ling SW, et al. Development of [^{225}Ac]Ac-PSMA-I&T for targeted alpha therapy according to GMP guidelines for treatment of mCRPC. *Pharmaceutics.* 2021;13:715.
9. Weineisen M, Schottelius M, Simecek J, et al. ^{68}Ga- and ^{177}Lu-Labeled PSMA I&T: optimization of a PSMA-targeted theranostic concept and first proof-of-concept human studies. *J Nucl Med.* 2015;56:1169–1176.
10. Kunert JP, Müller M, Günther T, et al. Synthesis and preclinical evaluation of novel ^{99m}Tc-labeled PSMA ligands for radioguided surgery of prostate cancer. *EJNMMI Res.* 2023;13:2.
11. Yusufi N, Wurzer A, Herz M, et al. Comparative preclinical biodistribution, dosimetry, and endoradiotherapy in metastatic castration-resistant prostate cancer using ^{19}F/^{177}Lu-rhPSMA-7.3 and ^{177}Lu-PSMA I&T. *J Nucl Med.* 2021;62:1106–1111.
12. Bolch WE, Jokisch D, Zankl M, et al.; on behalf of ICRP. ICRP publication 133: the ICRP computational framework for internal dose assessment for reference adults: specific absorbed fractions. *Ann ICRP.* 2016;45:5–73.
13. Kesner AL, Carter LM, Ramos JCO, et al. MIRD pamphlet no. 28, part 1: MIRDcalc—a software tool for medical internal radiation dosimetry. *J Nucl Med.* 2023;64:1117–1124.
14. Ruigrok EAM, Tamborino G, de Blois E, et al. In vitro dose effect relationships of actinium-225- and lutetium-177-labeled PSMA-I&T. *Eur J Nucl Med Mol Imaging.* 2022;49:3627–3638.
15. Kiess AP, Minn I, Chen Y, et al. Auger radiopharmaceutical therapy targeting prostate-specific membrane antigen. *J Nucl Med.* 2015;56:1401–1407.
16. Thiele NA, Brown V, Kelly JM, et al. An eighteen-membered macrocyclic ligand for actinium-225 targeted alpha therapy. *Angew Chem Int Ed Engl.* 2017;56:14712–14717.
17. Sartor O, de Bono J, Chi KN, et al.; VISION Investigators. Lutetium-177-PSMA-617 for metastatic castration-resistant prostate cancer. *N Engl J Med.* 2021;385:1091–1103.
18. Kalidindi TM, Lee SG, Jou K, et al. A simple strategy to reduce the salivary gland and kidney uptake of PSMA-targeting small molecule radiopharmaceuticals. *Eur J Nucl Med Mol Imaging.* 2021;48:2642–2651.
19. Wurzer A, Pollmann J, Schmidt A, Reich D, Wester HJ, Notni J. Molar activity of Ga-68 labeled PSMA inhibitor conjugates determines PET imaging results. *Mol Pharm.* 2018;15:4296–4302.
20. Davis IA, Glowienka KA, Boll RA, et al. Comparison of ^{225}actinium chelates: tissue distribution and radiotoxicity. *Nucl Med Biol.* 1999;26:581–589.
21. Meyer C, Stuparu A, Lueckerath K, et al. Tandem isotope therapy with ^{225}Ac- and ^{177}Lu-PSMA-617 in a murine model of prostate cancer. *J Nucl Med.* 2023;64:1772–1778.
22. Rupp NJ, Umbricht CA, Pizzuto DA, et al. First clinicopathologic evidence of a non-PSMA-related uptake mechanism for ^{68}Ga-PSMA-11 in salivary glands. *J Nucl Med.* 2019;60:1270–1276.
23. Müller M, Lucaroni L, Favalli N, et al. Discovery of glutamate carboxypeptidase III ligands to compete the uptake of [^{177}Lu]Lu-PSMA-617 in healthy organs. *J Med Chem.* 2024;67:8247–8260.
24. Rousseau E, Lau J, Kuo HT, et al. Monosodium glutamate reduces ^{68}Ga-PSMA-11 uptake in salivary glands and kidneys in a preclinical prostate cancer model. *J Nucl Med.* 2018;59:1865–1868.
25. Roy J, Warner BM, Basuli F, et al. Comparison of prostate-specific membrane antigen expression levels in human salivary glands to non-human primates and rodents. *Cancer Biother Radiopharm.* 2020;35:284–291.
26. Schwartz J, Jaggi JS, O'Donoghue JA, et al. Renal uptake of bismuth-213 and its contribution to kidney radiation dose following administration of actinium-225-labeled antibody. *Phys Med Biol.* 2011;56:721–733.
27. Perey M, Chevallier A. Distribution of element 87, francium, in tissues of the normal rat [In French]. *C R Seances Soc Biol Fil.* 1951;145:1205–1207.
28. Liubchenko G, Böning G, Zacherl M, et al. Image-based dosimetry for [^{225}Ac]Ac-PSMA-I&T therapy and the effect of daughter-specific pharmacokinetics. *Eur J Nucl Med Mol Imaging.* 2024;51:2504–2514.
29. Hooijman EL, Radchenko V, Ling SW, et al. Implementing Ac-225 labelled radiopharmaceuticals: practical considerations and (pre-)clinical perspectives. *EJNMMI Radiopharm Chem.* 2024;9:9.